Ordered patterns of liquid crystal toroidal defects by microchannel confinement

Myung Chul Choi*†‡§¶, Thomas Pfohl*†‡§‖, Zhiyu Wen**, Youli Li*††, Mahn Won Kim*¶††, Jacob N. Israelachvili*†‡‡, and Cyrus R. Safinya*†‡§††

*Materials Research Laboratory and Departments of †Materials, ‡Physics, §Molecular, Cellular, and Developmental Biology, and ‡‡Chemical Engineering, University of California, Santa Barbara, CA 93106; ¶Department of Physics, Korea Advanced Institute of Science and Technology, Daejon 305-701, Korea; ‖Department of Applied Physics, University of Ulm, D-89069 Ulm, Germany; and **College of Optoelectronic Engineering, Chongqing University, Chongqing 400044, China

Contributed by Jacob N. Israelachvili, October 25, 2004

In this article we present experimental results demonstrating an approach to controlling the size and spatial patterning of defect domains in a smectic liquid crystal (LC) by geometric confinement in surface-modified microchannels. By confining the LC 4′-octyl-4-cyanobiphenyl in μm-sized rectangular channels with controlled surface polarity, we were able to generate defect domains that are not only nearly uniform in size but also arranged in quasi-2D ordered patterns. Atomic force microscopy measurements revealed that the defects have a toroidal topology, which we argue is dictated by the boundary conditions imposed by the walls of the microchannel. We show that the defects can be considered to be colloidal objects, which interact with each other to form ordered patterns. This method opens the possibility for exploiting the unique optical and rheological properties associated with LC defects to making new materials. For example, the control of the shape, size, and spatial arrangement of the defects at the mesoscale suggests applications in patterning, templating, and when extended to lyotropic LCs, a process leading to uniform-sized spherical particles for chemical encapsulation and delivery.

Smectic (Sm) liquid crystals (LCs) are composed of elongated molecules that are aligned and arranged in layers. Local disruptions in the orientational, positional (layering), or morphological (bending) order in a Sm LC result in defects, which, when observed under crossed polarizers, exhibit complex textural patterns. The texture, which results from the highly anisotropic polarization of the molecules, has been extensively characterized and categorized based on the type of the LC structure (1–5). Understanding and controlling defects in LCs are important to many technological applications (e.g., displays and optical switches). Because the defects are considered to be anomalies in the LC structure, general efforts have been directed at minimizing or annealing the defects, including by using microstructures (grooves and gratings) (6–8). However, defect domains possess unique rheological and optical properties, which could potentially be exploited to make novel materials. The prerequisite for doing so would be the control of the type, size, and spatial distribution of the defects, which had not been well addressed in previous studies.

In this article we present experimental results demonstrating the control of the size and spatial distribution of toroidal defects in the Sm LC 4′-octyl-4-cyanobiphenyl (8CB) by using surface-modified microchannels. By changing the depth and width of the μm-scale channels with a controlled surface polarity, we were able to generate focal conic defects that are not only nearly uniform in size but also arranged in 2D ordered patterns. This process is analogous to colloidal crystallization, except here the "colloids" are the "soft" μm-sized defects within the LC. In addition, whereas the ordering in colloids is caused by interparticle interactions, here the defect ordering results from the competition between the boundary conditions and the elasticity of the Sm phase.

Materials and Methods

The microchannels were fabricated on (100) Si wafers by using photolithography and reactive ion etching techniques. The microchannels have a rectangular cross section with different widths and depths, which are the confining dimensions. The length of the channels is 1 mm. To control the surface polarity (hydrophobic-hydrophilic balance), the channels were coated with a layer of cationic polymer polyethyleneimine (PEI) as described (9). The uncoated clean Si surface was hydrophilic and negatively charged, and the water contact angle was measured to be $\theta_w < 5°$, whereas for PEI-coated surfaces the contact angle was θ_w (PEI) $\approx$20–30°. Thus the PEI-coated surface can be considered as predominantly hydrophilic but partially hydrophobic. The exact nature of this balance turns out to be very important for the formation of ordered LC defects in the microchannels. For comparisons studies, we coated flat Si substrates with a layer of octadecyltrichlorosilane (OTS) by using the polydimethylsiloxane contact printing stamp technique to create a fully hydrophobic surface [θ_w (OTS) $\approx$90°] (9).

8CB was purchased from BDH (Merck) and exists at room temperature as a viscous fluid. The 8CB sample was introduced into the microchannels by using a microinjector (Eppendorf) system. The channels were filled to the top with 8CB under an optical microscope; hence the film thickness was approximately equal to the depth of the channels. During sample loading, the microchannel substrate was heated to a temperature above the nematic-isotropic transition temperature (40.5°C) to facilitate the flow of 8CB into the channels. The substrate was then fast-cooled to room temperature at which the 8CB is in the Sm phase ($T_{\text{nematic-smectic A}} = 33.5$°C) (10).

Polarized microscopy measurements were conducted with a Nikon Microphot-FX upright microscope equipped with a charge-coupled device video camera and with high-resolution digital and film cameras. Atomic force microscopy (AFM) measurements were done by using a Digital Instruments (Santa Barbara, CA) multimode Nanoscope scanning probe microscope in the tapping mode.

Results

Polarized Microscopy. We show in Fig. 1 a series of optical microscopy images (under crossed polarizers) of the ordered defects confined in rectangular Si microchannels with different widths (20, 10, and 5 μm, left to right) and depths (10 and 5 μm, top to bottom). The corresponding microchannel samples are shown schematically in Fig. 1. The circular and semicircular objects in the images are focal conic defects characteristic of SmA LCs (1, 2, 4), which are composed of elongated molecules

Abbreviations: LC, liquid crystal; Sm, smectic; 8CB, 4′-octyl-4-cyanobiphenyl; PEI, polyethyleneimine; OTS, octadecyltrichlorosilane; AFM, atomic force microscopy.

††To whom correspondence may be addressed. E-mail: safinya@mrl.ucsb.edu, youli@mrl.ucsb.edu, or mwkim@kaist.ac.kr.

www.pnas.org/cgi/doi/10.1073/pnas.0407925101

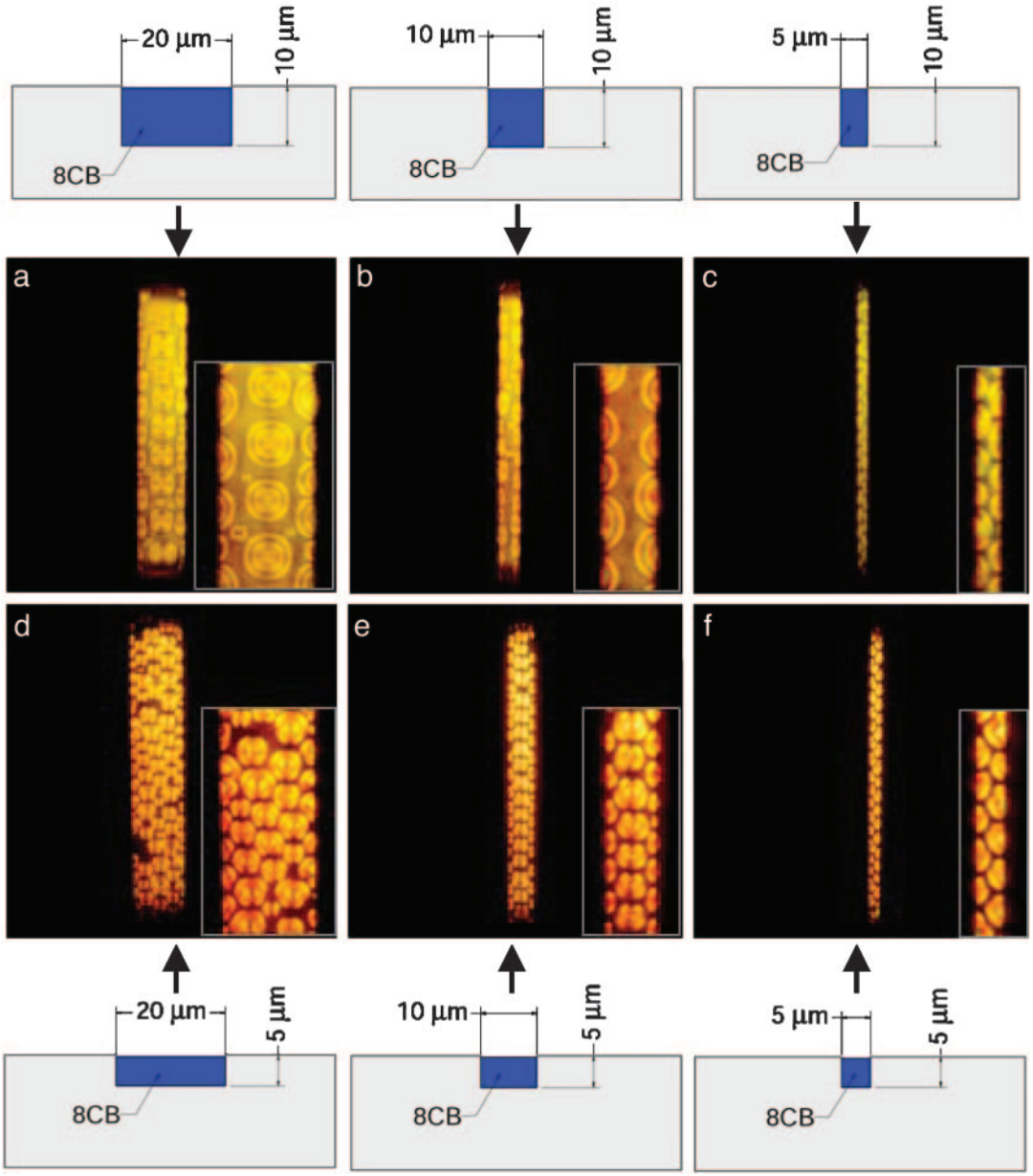

Fig. 1. Polarized light microscopy images of ordered focal conic defects of Sm 8CB in surface-modified microchannels (*Inset* images are magnified ×2), with corresponding schematic drawings shown above and below the images. From left to right, the widths of the channels are 20, 10, and 5 μm. In *a–c*, the channel depth is 10 μm. In *d–f*, the depth is 5 μm. (Magnification: ×400.)

that exhibit long-range orientational order and are arranged in stacked liquid layers. The light intensity variation (texture) within a defect domain originates from the change in orientation of the optically anisotropic rod-like 8CB molecule, which has a high birefringence $\Delta n(n_{\parallel} - n_{\perp}) = 0.157$ at 27°C (11). In a focal conic defect domain the optical axes of the 8CB molecules are oriented radially; thus when observed under crossed polarizers, the defect has a fan-shaped pattern with crossed extinction stripes in each domain. It is clear that the defects shown in Fig. 1 have the focal conic characteristics.

The images in Fig. 1 show several remarkable features. First, it appears that the defects in the microchannels adopt well defined sizes, with the average diameter of the circular defect approximately equal to the critical dimension (smaller of the depth or width) of the channel. This defect size selection rule is evident as the channel depth is decreased from 10 μm (Fig. 1 *a* and *b*) to 5 μm (Fig. 1 *d* and *e*) for the 10-μm (Fig. 1 *b* and *e*) and 20-μm (Fig. 1 *a* and *d*) channels. At constant channel depth the defect size remains constant as the channel width is varied (compare Fig. 1 *c–e* at 5-μm depth with Fig. 1 *a* and *b* at 10-μm depth). Second, the defects appear to be arranged in quasiperiodic lattices with different symmetries, such as the finite-size 2D body-centered cell shown in Fig. 1*e*. The patterning of the defects is directly controlled by the width of the channel. Moreover, at the side walls of the channel, only half-sized defects are seen. The defect ordering shown in Fig. 1, although imperfect, is highly persistent and can be observed over the entire length (1 mm) of the microchannel.

The surface properties of the Si microchannels play a crucial role in the formation of the ordered LC defect patterns. It is known that the 8CB molecules, which are composed of a hydrophilic polar cyano head group and a hydrophobic alkyl tail

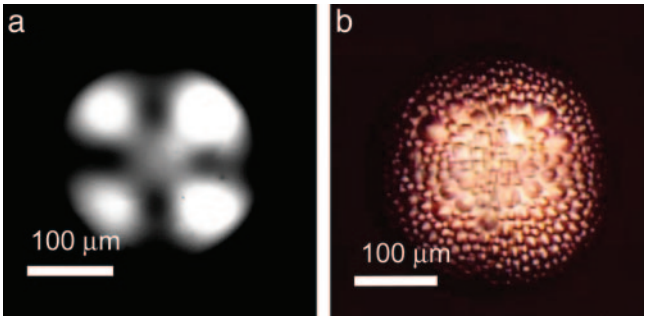

Fig. 2. Polarized microscopy images of 8CB droplets on flat Si surfaces with different surface polarities. (*a*) An 8CB droplet on a hydrophobic, OTS-coated flat Si surface. The texture is consistent with a giant multilayered onion-like structure. (*b*) An 8CB droplet on a hydrophilic, PEI-coated flat Si surface. The 8CB droplet is densely populated by toroidal defects that have a large size distribution.

group, adopt different orientations depending on the polarity of the surface (12). For completely hydrophobic surfaces the 8CB will adopt a homeotropic orientation in which the rod-like 8CB molecules are aligned normally to the surface. On hydrophilic surfaces the 8CB molecules prefer a planar orientation in which they align parallel to the surface. Therefore, by changing the surface polarity one can control the boundary conditions of the defects.

To demonstrate the effects of surface treatment on the LC defect structures, we show polarized microscope images of two lens-shaped 8CB droplets on flat (no channel) OTS/Si (Fig. 2*a*) and PEI/Si surfaces (Fig. 2*b*). The droplet on the hydrophobically rendered OTS/Si surface shows a single fan-shaped pattern consistent with a multilayered spherulitic structure (''onion''). The droplet on the PEI/Si surface, however, shows a proliferation of small, polydisperse defects. In contrast, 8CB on the hydrophilic, uncoated Si surface spreads and does not form a stable droplet. In the OTS-coated channels, the 8CB molecules align normally to the bottom surface of the channel and form a homogenous, defect-free SmA LC film. In uncoated Si channels defects also appear but they are polydispersed and the pattern is much less ordered. We observed the ordered patterns of uniformly sized defects only in PEI-coated channels.

AFM. The internal structure of the focal conic defect in a Sm LC can adopt one of two morphologies shown in Fig. 3 (4). Fig. 3*a* shows a spherulite-like defect, which has a positive Gaussian curvature ($1/R_1R_2 > 0$, where R_1 and R_2 are the principal radii in two orthogonal directions) and an onion-like multilayer structure (1, 2, 4). Fig. 3*b* shows a torus-like structure, which has a negative Gaussian curvature ($1/R_1R_2 < 0$) with a saddle-splay

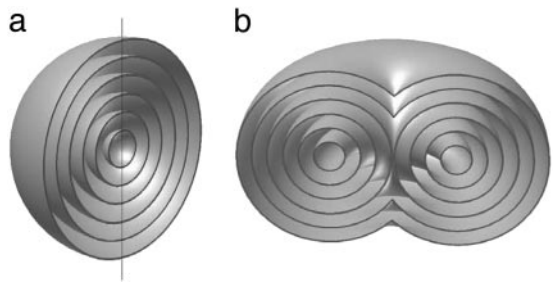

Fig. 3. Illustrations of the two types of LC defect structure. (*a*) An onion-like spherulite. (*b*) A toroidal defect. The surfaces in the drawings represent layers of 8CB molecules, which are oriented along the surface normally.

cross section. It is difficult to differentiate these two types of objects in the microchannels based on defect texture alone because both are circular in appearance under crossed polarizers. However, one may readily distinguish these two types of defects from surface topography.

To probe the surface topography of the defect domains we performed AFM measurements on Sm 8CB samples in a free droplet (Fig. 2*b*) and as confined in a microchannel. Fig. 4*a* shows the surface topographic image of a circular defect near the center of a 20-μm-wide, 10-μm-deep microchannel. The image data and the corresponding height traces (Fig. 4 *a* and *c*) unambiguously confirm that the defect is a funnel-shaped toroid. Another interesting feature in Fig. 4*a* is the ripple-like ridges near the channel side wall and in between two defects. They were likely formed to compensate for the curvature of the funnel dip and to maintain constant surface tension. In comparison, an image of a lens-shaped 8CB droplet on a flat PEI-coated surface is shown in Fig. 4*b*, with the corresponding height trace shown in Fig. 4*d*. The image shows multiple funnel-shaped toroidal defects with a large size distribution compared with those in the microchannels.

Discussion

The boundary conditions in the microchannels favor the formation of toroidal defects. Because the defects terminate at the bottom and/or the side walls of the PEI-coated microchannel, we expect that, as is observed experimentally (Fig. 1), the defect size will be limited by the smaller of the two geometric dimensions of the channel, namely the width and depth (assuming the channel is filled to the top). To understand the interactions of a toroidal defect with the side and bottom walls of the microchannel, let us consider the orientation of the 8CB molecules at various points on a toroidal defect as shown in Fig. 4*e*. The hydrophilic cyano group in the 8CB molecule prefers a planar orientation at the 8CB–PEI interface. Therefore the Sm director (surface normal of the layers) should run parallel with the substrate at the bottom or side walls of the channel. At the air–LC interface, however, the molecules prefer a homeotropic orientation, which would require that the Sm director be perpendicular to the substrate plane. These opposing demands at the top and bottom interfaces of the 8CB film in the microchannel can be reconciled by adopting a toroidal topology. Furthermore, because the side walls are perpendicular to the bottom, only a toroid that has been cut open would satisfy the boundary condition that the molecules be tangential at both surfaces, as observed experimentally. Fig. 4*f* shows a model of the ordered toroidal defect domains in a microchannel as shown in Fig. 1*a*.

The ordering of the uniform defect domains into quasi-periodic patterns can be qualitatively understood by considering the elastic and interfacial energies. The toroidal defects that result from a combination of boundary layer conditions with lower surface energies have stored elastic energy and can essentially be considered as ''hard'' objects, meaning that they are much stiffer in comparison to the bulk 8CB LC. Defect domains interact with each other through long-range elastic interactions mediated by the connecting Sm layers. When the concentration of defects becomes sufficiently large, the distribution of the defects into ordered patterns becomes energetically favorable because it lowers the elastic distortion energy in regions between defects. Thus, whereas on the local nanometer scale the material behaves as a quasi-1D solid because of the LC order, on the μm scale the microchannel-confined LC undergoes a 2D colloidal crystallization process in which the colloids are the μm-size defects within the LC. Clearly, a detailed theoretical understanding of the size selection and spatial ordering of the defects must take

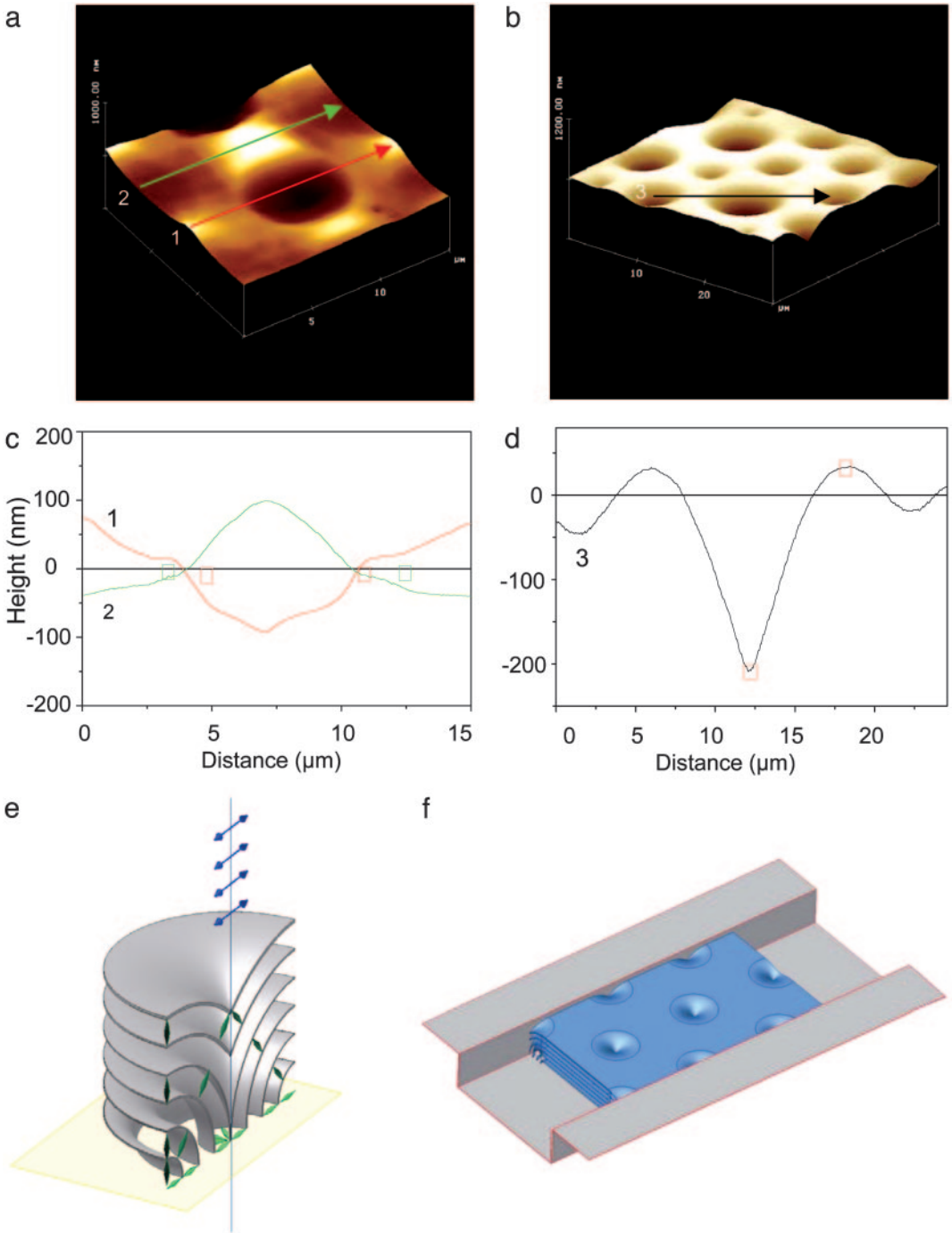

Fig. 4. AFM data and model of LC defects. (*a*) AFM image of an 8CB defect domain in a 20-μm-wide, 10-μm-deep microchannel, showing the toroidal topography. (*b*) AFM image of an area on an unconfined 8CB droplet populated by polydispersed toroidal defects. The droplet was formed on a flat PEI-coated Si surface. (*c* and *d*) Surface profile traces taken from the AFM images shown in *a* and *b* at positions marked by arrows numbered 1–3. (*e*) A central cutout view of a toroidal defect. The 8CB molecules are shown as green double cones, which change from a planar orientation at the bottom to the homeotropic orientation at the top. (*f*) Model of an ordered pattern of toroidal defects in a microchannel, which is consistent with the images shown in Fig. 1.

into account the interplay between surface and bulk elastic energies.

The patterning of uniform-sized defects described here offers tantalizing hints to the novel physical properties and possible applications of this material. In terms of its mechanical properties, it is expected that the ordered defects will behave like a quasi-2D solid with an in-plane elastic modulus, analogous to colloidal crystals (13). The ordering of the highly birefringent defects opens the way to harnessing the unique nonlinear optical properties in the LC defect domain. It should be possible to use the ordered patterns as templates for new materials. Furthermore, the same mechanism that is responsible for ordering the defects should also apply to polymeric and lyotropic LCs, which would open up many other application possibilities. For example, it is possible to apply the methodology to create uniform and ordered multilamellar lipid vesicles, which can be used as chemical and gene carriers (14, 15). The demonstrated ability to control not only the size of the defects but also their spatial order

(pattern) may be particularly important for their potential technological applications.

This work was supported by National Institutes of Health Grant GM-59288, National Science Foundation Grants DMR-0203755, CTS-04044444, and CTS-0103516, and Office of Naval Research Grant N00014-00-1-0214. M.W.K. gratefully acknowledges support by Korea Institute of Science and Technology Evaluation and Planning Grants I-03-064 and IMT-2000-B3-2. Support for the Materials Research Science and Engineering Center at the Materials Research Laboratory at the University of California, Santa Barbara, is provided by National Science Foundation Grant DMR-0080034.

1. de Gennes, P.-G. & Prost, J. (1993) *The Physics of Liquid Crystals* (Clarendon, Oxford), 2nd Ed.
2. Collings, P. J. & Hird, M. (2001) *Introduction to Liquid Crystals: Chemistry and Physics* (Taylor & Francis, London)
3. Ouchi, Y., Takanishi, Y., Takezoe, H. & Fukuda, A. (1989) *Jpn. J. Appl. Phys.* **28,** 2547–2551.
4. Boltenhagen, P., Lavrentovich, O. D. & Kleman, M. (1992) *Phys. Rev. A* **46,** R1743–R1746.
5. Coleman, D. A., Fernsler, J., Chattham, N., Nakata, M., Takanishi, Y., Körblova, E., Link, D. R., Shao, R.-F., Jang, W. G., Maclennan, J. E., *et al.* (2003) *Science* **301,** 1204–1211.
6. Keller, S. L., Warriner, H. E., Safinya, C. R. & Zasadzinski, J. A. (1997) *Phys. Rev. Lett.* **78,** 4781–4784.
7. Kawata, Y., Takatoh, K., Hasegawa, M. & Sakamoto, M. (1994) *Liq. Crystallogr.* **16,** 1027–1036.
8. Flanders, D. C., Shaver, D. C. & Smith, H. I. (1978) *Appl. Phys. Lett.* **32,** 597–598.
9. Pfohl, T., Kim, J. H., Yasa, M., Miller, H. P., Wong, G. C., Bringezu, F., Wen, Z., Wilson, L., Kim, M. W., Li, Y. & Safinya, C. R. (2001) *Langmuir* **17,** 5343–5351.
10. Davidov, D., Safinya, C. R., Kaplan, M., Daha, S. S., Schaetzing, R., Birgeneau, R. J. & Litster, J. D. (1979) *Phys. Rev. B* **19,** 1657–1663.
11. Dunmur, D. A., Manterfield, M. R., Miller, W. H. & Dunleavy, J. K. (1978) *Mol. Crystallogr. Liq. Crystallogr.* **45,** 127–144.
12. Volovik, G. E. & Lavrentovich, O. D. (1983) *Sov. Phys. JETP* **58,** 1159–1166.
13. Gasser, U., Weeks, E. R., Schofield, A., Pusey, P. N. & Weitz, D. A. (2001) *Science* **13,** 258–262.
14. Safinya, C. R. (2001) *Curr. Opin. Struct. Biol.* **11,** 440–448.
15. Radler, J. O., Koltover, I., Salditt, T. & Safinya, C. R. (1997) *Science* **275,** 810–814.